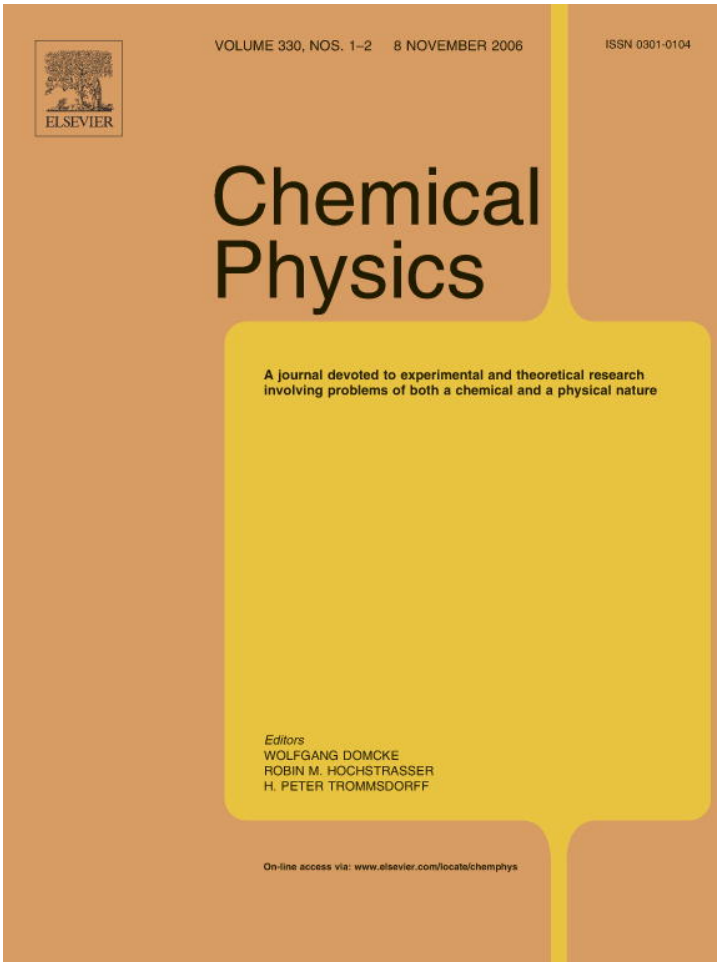

Available online at www.sciencedirect.com
ScienceDirect
Chemical Physics 330 (2006) 26–42
Chemical Physics
www.elsevier.com/locate/chemphys

Theoretical, *ab initio* and DFT, study of the structure and vibrational analysis of Raman, IR and INS spectra of $(CH_3)_3SiNCO$

M.P. Fernández-Liencres [a,*], A. Navarro [a], A. Ben Altabef [b,1], J.J. López-González [a], M. Fernández-Gómez [a], G.J. Kearley [c]

[a] *Department of Physical and Analytical Chemistry, University of Jaén, 23071 Jaén, Spain*
[b] *Instituto de Química Física, Facultad de Bioquímica, Química y Farmacia, Universidad Nacional de Tucumán, San Lorenzo 456, 4000 S.M. de Tucumán, Argentina*
[c] *Department of Radiation, Radionuclides & Reactors, Faculty of Applied Sciences, Delft University of Technology, Mekelweg 15, 2629 JB Delft, The Netherlands*

Received 25 April 2005; accepted 25 July 2006
Available online 28 July 2006

Abstract

The molecular geometry for trimethylsilylisocyanate ($(CH_3)_3SiNCO$) has been calculated at MP2 and DFT/B3LYP and DFT/B3PW91 methods, and using the 6-31G*, 6-311G**, 6-311++G**, cc-pVDZ and cc-pVTZ basis sets. The equilibrium structure of the molecule, linear or bent as concerns the –SiNCO moiety, was found to rely on the method employed. The potential energy surface of –SiNC bending has been investigated by quantum mechanical ab initio calculations at MPn ($n = 2$–4) and QCISD(T) levels of theory with the cc-pVTZ basis set. This large amplitude bending motion (the υ_{24} mode) was determined to be very anharmonic, with a low barrier to linearity of the SiNCO skeleton of ~4–25 cm^{-1}. New vapour and liquid IR, liquid Raman spectra and, for first time, INS spectrum have been recorded, and a complete vibrational assignment has been performed. INS data have allowed to assign two modes at 674 cm^{-1} and 141 cm^{-1} which, so far, have been considered as silent, i.e. A_2, since previous authors have used a frame of C_{3v} symmetry for this system. The intermolecular interactions show to have little effect on the torsional region (below 250 cm^{-1} in INS spectrum) and the isolated-molecule approximation works well in that region. A normal coordinate analysis has been carried out by scaling the force fields calculated at MP2/6-311++G** and B3LYP/cc-pVDZ levels of theory using the scaled quantum mechanical force field (SQMFF) methodology. In order to get the best possible agreement between calculated and observed vibrational wavenumbers, the scale factors were refined by least squares yielding a final r.m.s. of ≈7 cm^{-1}.

Keywords: Trimethylsilylisocyanate; Vibrational analysis; Structure; Ab initio; DFT; Infrared; Raman; INS

1. Introduction

Over the last 50 years, the knowledge and understanding of organosilane compounds has increased considerably, and these materials now have applications in nearly all aspects of modern industry (in the clinical testing, pharmaceutical, medical, chemical, research and manufacturing industries) [1,2], trimethylsilyl moiety being the most common protecting group used in organic synthesis [3,4]. Isocyanates are widely used in the manufacture of flexible and rigid foams, fibres, coatings such as paints and varnished, in the automobile industry and building insulation materials but they also have important effects for the health and are classified as potential human carcinogens. Recent studies have shown that $(CH_3)_3SiNCO$ has applications as

* Corresponding author.
E-mail address: liencres@ujaen.es (M.P. Fernández-Liencres).
[1] Member of the National Research Council of R. Argentina.

0301-0104/$ - see front matter © 2006 Elsevier B.V. All rights reserved.
doi:10.1016/j.chemphys.2006.07.033

intermediate in the synthesis of important phosphorylated isocyanates compounds [5,6].

The structure and vibrational spectrum of $(CH_3)_3SiNCO$ have been studied in the past. The molecular structure of silylisocyanate exhibits a wide range of bond angles at nitrogen depending on the attached atom, the phase and the technique employed. In 1966, an electron diffraction study of $(CH_3)_3SiNCO$ [7] suggested a bent skeleton with a Si–N–C angle of 150°, but there were large uncertainties in the parameters reported. A microwave study [8] showed, 6 years later, a value of 180° for this angle although it was not able to define the structure in this case, as the vibrational ground state molecule gave rise to a pattern of lines indistinguishable from that of a symmetric top. A new determination of the molecular structure of $(CH_3)_3SiNCO$ by electron diffraction was made by Cradock et al. [9], in 1985, yielding apparent deviations from linearity of the SiNCO skeleton (SiNC 156.9° and NCO 165.8° bond angles). The value obtained by electron diffraction [9] for the Si–N–C angle can be understood taking into account that the low value of the bending frequency SiNC causes a large number of excited vibrational states to be populated at room temperature. The location of the energy levels relative to the SiNC bending potential energy function should be accomplished in order to go deeper in this matter and it is beyond of the scope of this work.

Recently, comparative theoretical studies of the structures of different silane compounds, including the $(CH_3)_3SiNCO$ molecule, have been performed by Palmer and Nelson [10] and Zanchini and Crispini [11]. In these studies, the optimum structural parameters were determined at the second-order Møller–Plesset level of theory (MP2) using basis set of triple zeta valence *plus* polarisation (TZVP) in the first case and the 6-311G** basis set and, also B3LYP/6-311G(2df,2pd) level, in the second study. MP2/TZVP values for SiNC and NCO angles turned out to be 156° and 177.3°, respectively, while MP2/6-311G** and B3LYP/6-311G(2df,2pd) results also indicate a bent structure.

As discussed by Koput when studying a related system, H_3SiNCO, in reference 12, differences between theoretical and experimental values can be due to errors inherent in either the theoretical and experimental procedures. To attain a sufficient accuracy for bonds involving second-row atoms a larger basis set, beyond triple-zeta quality, is necessary [13].

The anharmonicity of SiNC bending potential can be tested by studying its potential energy surface. However, from a previous papers on the energy surface of H_3SiNCO [12], it is apparent that reliable results for molecules of this type can only be obtained using extensively correlated wavefunctions, beyond the MP2 level, and large one-particle basis sets, including higher polarization functions. It seems that the coupled cluster method and Quadratic Configuration Interaction (QCI) with a large basis set of spdf quality can be the lowest levels of theory for which a compromise between the desired accuracy and computational feasibility can be reached, as far as the potential energy surface of large-amplitude motion is concerned.

The coupled cluster methods and Quadratic Configuration Interaction represent a higher-level treatment of electron correlation beyond MP4, usually providing even greater accuracy. Both methods are very similar and both iteratively include the effects of single and double substitution, effectively adding higher order terms than MP4, and can optionally include triples and quadruples. The preliminary studies showed that cc-pVTZ is the best basis set considering computational time and our available hardware facilities.

Turning to the vibrational spectrum, the first infrared spectrum of $(CH_3)_3SiNCO$ was recorded by Thayer and Strommen [14] who focussed their investigation on the bending and two stretching modes of the pseudohalogen (NCO) group and the Si–N stretching and also reported previous Raman data from Ref. [15]. Similarly, Durig et al. [16] recorded the IR and Raman spectra, assigning most of the vibrational modes by comparing them to those of similar molecules, but without any force field calculation. One year later, they carried out a modified simple force field [17] assuming a molecular structure under C_{3v} symmetry and on the basis of the structural results from the microwave study [8]. The initial values for the force constants in the refinement procedure were taken from $(CH_3)_3SiCl$ except for the N–C and C–O force constants that were taken from methylisocyanate and held constant during the fitting process.

None of the previous studies about the vibrational spectrum of $(CH_3)_3SiNCO$ [14–17] have provided a complete vibrational assignment and some of the low-frequency vibrations remain unassigned. Furthermore, the vibrational study was limited because under the C_{3v} point-group symmetry assumed for the vibrational analysis there were optically-inactive modes that were not assigned from the IR and Raman optical techniques.

In the present study, in order to check the anharmonicity of SiNC bending potential and also to study the vibrational dynamics of $(CH_3)_3SiNCO$ we have performed geometry optimizations with ab initio, MP2, and DFT methods, in combination with different basis sets. Taking into account the optimized parameters for several fixed values of SiNC angle at MP2/cc-pVTZ level, the potential energy surface of trimethylsilyl isocyanate has been investigated with MP3, MP4 and QCISD(T) method. New IR and Raman spectra have been recorded and, for the first time, the inelastic neutron scattering (INS) spectrum has also been obtained, this being particularly useful in the assignment of the optically-silent modes and the low-energy region where most of uncertainties arise. In INS spectroscopy it is possible to compare observed and calculated spectra directly because the intensities are simply related to atomic displacements and peak shapes can also be calculated.

The vibrational spectrum has been studied by scaling the MP2/6-311++G** and B3LYP/cc-pVDZ force fields with the method developed by Pulay et al. [18] that uses

non-redundant natural internal coordinates. The number of scale factors has been defined according to each type of natural internal coordinates, and the presence of the silicon atom has been considered for grouping these coordinates. Finally, in order to get the best possible agreement between calculated and observed wavenumbers, the scale factors were refined yielding a final r.m.s. of $\approx 7\ cm^{-1}$. With obtained results, we think that some of the patterns followed in the analysis and interpretation of the vibrational spectra of trimethylsilyl isocyanate could be useful for the vibrational study of other derivatives.

Furthermore, the examination of the torsion region ($120–250\ cm^{-1}$) in INS spectrum of trimethylsilylisocyanate is of special interest in order to shed some light on the inter- or intramolecular interactions that determine the rotational potential of the methyl groups in this system. The potential that describes the rotational dynamics of a methyl group is determined by intermolecular interactions with the neighbouring atoms, the magnitude of this potential being around $135–323\ cm^{-1}$. This represents a low rotational barrier [19]. The approximately exponential dependence of the tunnel effects on the height of the potential barrier makes the methyl group a highly sensitive probe of its chemical environment. Rotational tunnelling of methyl groups in molecular crystals provides a uniquely sensitive probe of intermolecular interactions and weak intramolecular interactions in the solid state. The observed tunnelling frequencies for a series of compounds for which crystallographic data at liquid helium temperature are known were reproduced by the rotational potential calculated from high level ab initio methods on single molecules. Parameterised van der Waals and Coulomb interactions were used to describe intermolecular interactions [20,21].

2. Experimental

The INS spectrum was obtained using TFXA spectrometer at the ISIS pulsed neutron source, in Rutherford Appleton Laboratory, Chilton, UK. This instrument has a fixed final energy determined by a Bragg reflection from a graphite analyser, and an energy resolution <2% of the energy transfer. The counting time for the sample was ≈12 h. The sample was loaded into a standard liquid-helium cryostat controlled at $T < 20$ K. The low temperature is required to sharpen the vibrational fundamental bands and to decrease the intensity of the phonon wings.

The IR spectrum was recorded, for the pure liquid, in a Bruker Vector 22 FT-IR spectrometer, equipped with a high intensity Globar source and a DGTS detector, using a Beckman cell with CsI windows. The gas phase spectrum was recorded using a 10 cm path cell, with CsI windows. The Raman spectrum was recorded at room temperature for the liquid sample using a Bruker FTRaman RFS100/S spectrometer equipped with a Nd:YAG laser (excitation line 1064 nm) and a liquid-nitrogen cooled germanium detector and using a quartz cell of path length of 5 mm. The spectral resolution was $1\ cm^{-1}$ in all the cases.

3. Computational details

The program GAUSSIAN 03 [22] was used to carry out the *ab inito* and DFT calculations running on a Digital Alpha Server 4100 and a IA64 HP Server rx2600. Calculations were performed using standard gradient techniques at the MP2 and DFT methods using the 6-31G*, 6-311G**, 6-311++G** standard split-valence basis set and, cc-pVDZ and cc-pVTZ basis sets of Dunning and coworkers [23–26]. In the case of the DFT methods Becke's hybrid exchange was used, B3, [27] and as correlation functionals the Lee–Yang–Parr non-local functional, LYP [28,29], and the gradient-corrected functional by Perdew and Wang [30], PW91, were chosen. Vibrational wavenumbers were calculated from analytical second derivatives to check the minimum of the potential energy surface.

The program CLIMAX [31] was used to calculate the INS spectral profile from the vibrational frequencies and atomic displacements resulting from the various ab-intio calculations. CLIMAX produces S(Q,/w/) intensities taking full account of the Debye-Waller factor for the fundamentals, overtones and combinations. The INS spectral intensities are calculated according to the theory given by Tomkinson et al. [32,33].

To study the shape of the potential energy function and the barrier to linearity of the SiNC angle, single point calculations were performed using cc-pVTZ basis set and several levels of theory, ranging from the Møller Plesset method up to full fourth order (MP4) and the quadratic configuration interaction method including a perturbational corrections for the effect of the connected triple excitations (CCSD(T) [34]).

In order to decide about what experimental molecular structure to choose, we have carried out a comparative analysis between the energy associated to the experimental structures and those optimized with 6-31G* and 6-311++G** basis sets at the MP2 level as well as with cc-pVTZ and cc-pVDZ basis sets from the hybrid DFT calculation by B3PW91 and B3LYP method respectively.

To obtain a complete description of the molecular motion involved in the normal modes the force constant matrix in Cartesian coordinates from Gaussian was transformed into the system of natural coordinates by using the non-commercial program package VIBRA [35], and the force field was scaled using the program ASYM40 [36]. Natural internal coordinates were used for the scaling procedure, as defined by Pulay et al. [37,38]. The scaling was made using the standard model developed by Pulay et al. [18] in which the diagonal force constants F_{ii} are multiplied by scale factors f_i, and the corresponding interaction constants F_{ij} are multiplied by $(f_i f_j)^{1/2}$. In the refinement process of scale factors these are adjusted to obtain best agreement with the experimental wavenumbers. Two initial sets of scale factors were used, firstly, starting from unity for all the scale factors, and secondly transferring those corresponding to the natural coordinates defined in this work and previously published and recommended in Ref.

[38,39] for the B3LYP/6-31G* method. The inverse experimental wavenumbers were used as weights for the vibrational modes in the fitting procedure, whereas zero weights were assigned to missing or uncertain wavenumbers. The potential energy distribution was subsequently calculated with the resulting SQM force field. These natural coordinates are shown in Table 1 and, the corresponding internal coordinates are shown in Fig. 1.

4. Structural results

In this study, the molecular structure of $(CH_3)_3SiNCO$ has been optimized at different levels of theory. A linear structure was predicted when using B3LYP and B3PW91 methods with 6-31G*, 6-311G** and 6-311++G** basis sets and MP2 method with 6-31G* basis set. However, MP2 with 6-311G**, 6-311++G**, cc-pVDZ and cc-pVTZ basis sets and DFT methods with cc-pVDZ and cc-pVTZ basis sets produce a bent structure with C_s symmetry.

According with the stated in the introduction, microwave results are at odds with electron diffraction's ones as concern Si–N–C and N–C–O angles. In order to decide about what experimental structure to choose, we have made a comparison between the energies associated to the optimized structures and the experimental ones. In all cases, the difference $(E_{exp.} - E_o^{theo.}) = \Delta E$, where $E_o^{theo.}$ means zero point corrected value, between such energy values is less for electron diffraction results, except in the case of MP2/6-31G*, wherein microwave results turn out to be nearer for the theoretical value. For instance, such a difference amounts to 3.6×10^{-3} hartree/particle for microwave structure in the case of MP2/6-311++G** whereas it rises to 2.02×10^{-3} hartree/particle for electron diffraction results. On the basis of this general behaviour, we adopt as the experimental molecular structure to be compared with the theoretical ones that obtained though electron diffraction, according to which the –Si–N–C–O moiety is bent.

The calculated geometrical parameters (bonds lengths and valence angles) obtained in the different calculations along with electron diffraction parameters from Cradock's work [9] are given in Table 2. It must be emphasised that in the case of the C_s symmetry the equivalent bond lengths and angles involving methyl groups have been averaged due their close similarity (differences <0.003 Å for Si–C and C–H bond distances and <0.2°, 1.2° and 0.6° for CSiC, CSiN and SiCH angles, respectively).

The results show that for all experimental studies [7–9] and all calculations performed in the present work there is a correlation between both N–C and C–O bond lengths,

Table 1
Natural internal coordinates of trimethylsilyl isocyanate

Number	Internal coordinates	Description
1–3	r_2, r_3, r_4	C–Si stretching
4–12	r_5, r_6, r_7, r_8, r_9, r_{10}, r_{11}, r_{12}, r_{13}	C–H stretching
13	r_1	Si–N stretching
14	r_{14}	N–C stretching
15	r_{15}	C–O stretching
16	$\varepsilon_2 + \varepsilon_4 + \varepsilon_3 - \gamma_2 - \gamma_4 - \gamma_3$	SiC_3 symmetric deformation
17	$2\varepsilon_2 - \varepsilon_4 - \varepsilon_3$	SiC_3 antisymmetric deformation
18	$\varepsilon_4 - \varepsilon_3$	SiC_3 antisymmetric deformation
19	$2\gamma_2 - \gamma_4 - \gamma_3$	SiC_3 rocking
20	$\gamma_4 - \gamma_3$	SiC_3 rocking
21	$\alpha_7 + \alpha_6 + \alpha_5 - \beta_7 - \beta_6 - \beta_5$	CH_3 symmetric deformation
22	$2\alpha_7 - \alpha_6 - \alpha_5$	CH_3 antisymmetric deformation
23	$\alpha_6 - \alpha_5$	CH_3 antisymmetric deformation
24	$2\beta_7 - \beta_6 - \beta_5$	CH_3 rocking
25	$\beta_6 - \beta_5$	CH_3 rocking
26	$\alpha_9 + \alpha_8 + \alpha_{10} - \beta_9 - \beta_8 - \beta_{10}$	CH_3 symmetric deformation
27	$2\alpha_9 - \alpha_8 - \alpha_{10}$	CH_3 antisymmetric deformation
28	$\alpha_8 - \alpha_{10}$	CH_3 antisymmetric deformation
29	$2\beta_9 - \beta_8 - \beta_{10}$	CH_3 rocking
30	$\beta_8 - \beta_{10}$	CH_3 rocking
31	$\alpha_{13} + \alpha_{12} + \alpha_{11} - \beta_{13} - \beta_{12} - \beta_{11}$	CH_3 symmetric deformation
32	$2\alpha_{13} - \alpha_{12} - \alpha_{11}$	CH_3 antisymmetric deformation
33	$\alpha_{12} - \alpha_{11}$	CH_3 antisymmetric deformation
34	$2\beta_{13} - \beta_{12} - \beta_{11}$	CH_3 rocking
35	$\beta_{12} - \beta_{11}$	CH_3 rocking
36	θ_1	SiNC bending
37	θ_2	NCO bending
38	$\tau_{5,3} + \tau_{6,3} + \tau_{7,3} + \tau_{5,4} + \tau_{6,4} + \tau_{7,4} + \tau_{5,14} + \tau_{6,14} + \tau_{7,14}$	CH_3 torsion
39	$\tau_{8,2} + \tau_{9,2} + \tau_{10,2} + \tau_{8,4} + \tau_{9,4} + \tau_{10,4} + \tau_{8,14} + \tau_{9,14} + \tau_{10,14}$	CH_3 torsion
40	$\tau_{11,2} + \tau_{12,2} + \tau_{13,2} + \tau_{11,3} + \tau_{12,3} + \tau_{13,3} + \tau_{11,14} + \tau_{12,14} + \tau_{13,14}$	CH_3 torsion
41	$\tau_2 + \tau_3 + \tau_4$	SiC_3 torsion
42	τ_1	SiNCO torsion

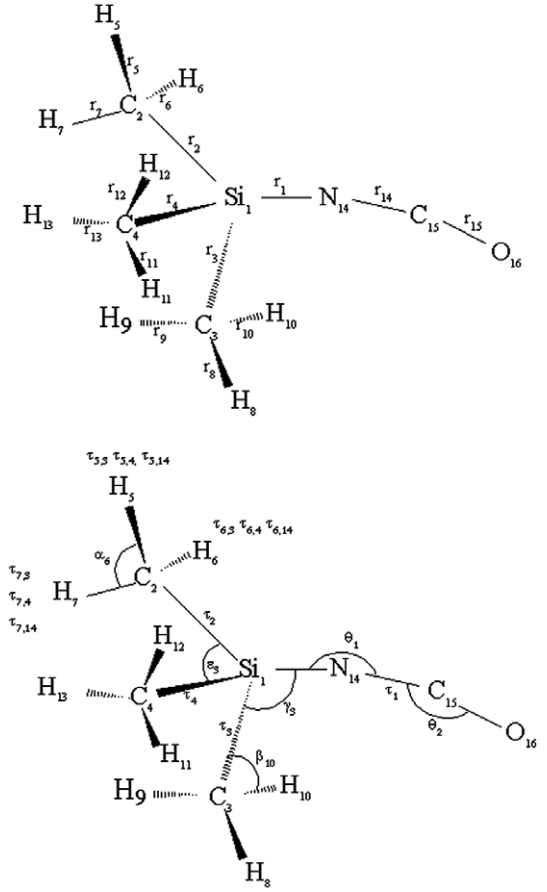

Fig. 1. Internal coordinates defined for the trimethylsilylisocyanate molecule.

the N–C bond distances (see Table 2) always being longer than C–O. Their values are similar to those found in SiH_3NCO from microwave: 1.199 and 1.174 Å [40] and electron diffraction: 1.216 and 1.164 Å [41], and in GeH_3NCO from microwave: 1.190 and 1.182 Å [42], respectively. Note that when comparing experimental [9] and calculated values, the MP2/cc-pVDZ method was found to calculate the longest N–C and Si–N distances with relative errors of 1.6% and 1.9% respectively.

For the Si–N bond length the calculations achieve good agreement with the experimental data, 1.740 Å [9]. This value somewhat longer than that found in SiH_3NCO, 1.703 Å by using electron diffraction and microwave techniques [40,41] as expected due to the electron-donating effects of three methyl substituents. This behaviour is in agreement with recent theoretical results that reproduce the experimentally observed trend of the Si–N bond length, showing a slight R-dependence in a series of silylisocyanates, R_3SiNCO (R = H, F, Cl, CH_3) in the order $CH_3 > H > Cl \approx F$ [11]. Considering the interatomic C–Si distances, all the calculated values show relative errors lower than 1.1% (in relation to the experimental value, 1.864 Å) and they are close to the corresponding microwave experimental data for the molecules CH_3SiH [43] (1.8668 Å) and $(CH_3)_3SiH$ [44] (1.868 Å), especially in the case of MP2/6-311G**, MP2/6-311++G** and MP2/cc-pVTZ methods.

The main disagreement between the optimized geometries at different levels of theory in $(CH_3)_3SiNCO$ and the experimentally determined by electron diffraction technique [9] is found for the Si–N–C and N–C–O angles that determine the linearity of this system. The results show that the level of theory, the use of polarized basis sets and, as show below, the type of correlation treatment, are decisive for reproducing the bent structure, both angles being calculated as bent for MP2/6-311G**, MP2/6-311++G**, MP2/cc-pVDZ, DFT/cc-pVDZ and DFT/cc-pVTZ methods. At the MP2 level, the Si–N–C and N–C–O angles are sensitive to improvements in the basis set, the 6-311++G** basis set leading to the best rms value for

Table 2
Comparison of experimental and calculated structural parameters for $(CH_3)_3SiNCO$ (distances in Å, angles in degrees, energy in Hartree)

Method	Basis set	Bond distances					Angles				$E_0 = E_{elec.} + ZPE$
		Si–C	Si–N	N=C	C=O	C–H	C–Si–C	Si–N–C	N–C–O	Si–C–H	
MP2	6-31 G*	1.874	1.745	1.206	1.192	1.094	111.4	179.9	180.0	111.0	−575.833900
	6-311G**	1.866	1.741	1.207	1.179	1.094	111.2	160.4	177.5	110.9	−576.051260
	6-311++G**	1.868	1.747	1.208	1.181	1.094	111.4	157.1	177.2	110.9	−576.061695
	cc-pVDZ	1.880	1.773	1.221	1.187	1.103	111.5	146.6	175.8	110.8	−575.930604
	cc-pVTZ	1.869	1.742	1.204	1.180	1.089	111.4	158.5	177.4	110.9	−576.270852
B3LYP	6-31G*	1.882	1.741	1.198	1.182	1.096	111.2	180.0	180.0	111.1	−577.274256
	6-311G**	1.877	1.742	1.193	1.173	1.094	111.2	180.0	179.9	111.0	−577.390184
	6-311++G**	1.877	1.745	1.193	1.175	1.094	111.4	180.0	180.0	111.0	−577.395470
	cc-pVDZ	1.885	1.761	1.201	1.180	1.102	111.4	166.4	178.2	110.9	−577.298013
	cc-pVTZ	1.877	1.741	1.191	1.173	1.109	111.3	170.3	178.9	111.0	−577.425678
B3PW91	6-31G*	1.879	1.739	1.197	1.180	1.096	111.2	179.8	180.0	111.1	−577.115560
	6-311G**	1.873	1.738	1.193	1.171	1.094	111.2	179.9	180.0	111.0	−577.223557
	6-311++G**	1.873	1.741	1.192	1.173	1.094	111.4	179.8	180.0	111.0	−577.228223
	cc-pVDZ	1.880	1.761	1.201	1.178	1.102	111.4	162.6	177.7	110.8	−577.143441
	cc-pVTZ	1.873	1.739	1.192	1.171	1.092	111.2	166.3	178.4	110.9	−577.258496
Experimental[9]		1.864	1.740	1.202	1.176	1.099	108.8	156.9	165.8	109.0	

angles (rms: 6.83°, see Table 3) and, there seems no necessity to increase the size of basis sets since 6-311++G** basis set results are very similar to those obtained with the larger basis cc-pVTZ as well as with TZVP published recently [10]. As regards the B3LYP and B3PW91 methods with cc-pVDZ and cc-pVTZ, the results indicate that B3PW91 gives smaller rms for both bond distance and angles than B3LYP method. Also it should be noted that the rms value for angles obtained from the B3LYP/cc-pVTZ calculation is the highest value without taking into account the rms value of 15.7° obtained from the all methods which reproduce linear structure (see Table 3).

The total molecular energy for the minimum calculated at each level of theory for $(CH_3)_3SiNCO$ has been corrected with the ZPE and appears collected in Table 2. These results clearly show that the bigger basis set used gives the lower the calculated energy value, regardless the method employed, and that B3LYP methods find deeper minima than B3PW91. In general, the lowest deviation between the experimental [9] and calculated structural parameters is obtained from MP2/6-311++G** and consequently this has been selected for the subsequent vibrational analysis of the trimethylsilylisocyanate compound.

The SiNC bending potential energy function has been determined by optimizing the structural parameters for several fixed values of the SiNC angle and the results are given in Table 4. The structural parameters were optimized using the MP2 method with cc-pVTZ basis set. Further geometry optimization, using a larger basis set or/and a higher level of theory, would involve, however, much larger computer resources and in view of the expense it was not attempted. At the MP2/cc-pVTZ level (see Table 4), the SiNCO skeleton is predicted to be bent at the minimum of the total energy, with the NCO group being slightly non-linear and in a trans-configuration. The SiC_m bond lengths are found to be essentially independent of the SiNC angle, while the bond lengths for the SiNCO skeleton are calculated to vary significantly with the SiNC angle. Thus, the SiN and NC bond lengths increase, while the CO bond length decrease non linearly with decreasing SiNC angle. The largest difference in the SiN bond length amounts to as much as 0.018 Å when the SiNC angle ranges from 180° to 140°.

To characterize the SiNC bending potential energy function, the dependencies of the energies on the Si–N–C angle have been investigated for each structure optimized at MP2/cc-pVTZ and, in addition, by single point calculations at MP3, MP4 and CCSD(T) method with cc-pVTZ basis. Results of calculation are given in Table 5. Then, the total energies were fitted with an analytical function, being chosen a quadratic potential with a Lorentzian hump [12],

Table 3
Root-mean square deviation between the experimental and calculated structural parameters and between observed and calculated wavenumbers at each level of theory for $(CH_3)_3SiNCO$

Method	Basis set	Bond distances	Angles	Wavenumbers
MP2	6-31G*	0.0103	15.73	120.8
	6-311G**	4×10^{-3}	7.24	97.0
	6-311++G**	6.1×10^{-3}	6.83	93.2
	cc-pVDZ	0.0215	8.50	99.8
	cc-pVTZ	6.1×10^{-3}	7.01	93.9
B3LYP	6-31G*	9.8×10^{-3}	15.74	84.2
	6-311G**	8.5×10^{-3}	15.71	68.4
	6-311++G**	8.7×10^{-3}	15.73	66.6
	cc-pVDZ	0.015	9.21	69.8
	cc-pVTZ	0.010	11.00	67.3
B3PW91	6-31G*	8.3×10^{-3}	15.68	90.9
	6-311G**	7.3×10^{-3}	15.71	76.3
	6-311++G**	7.3×10^{-3}	15.67	74.9
	cc-pVDZ	0.013	7.83	81.3
	cc-pVTZ	8×10^{-3}	9.24	74.0

Distances in Å, angles in degrees and wavenumbers in cm^{-1}.

Table 4
Optimized values of the structural parameters for $(CH_3)_3SiNCO$, determined for various assumed values of the SiNC angle at the MP2/cc-pVTZ level of theory

r (SiN) (Å)	1.7370	1.7375	1.7411	1.7417	1.7468	1.7546
r (NC) (Å)	1.2003	1.2010	1.2034	1.2038	1.2070	1.2116
r (CO) (Å)	1.1808	1.1804	1.1798	1.1798	1.1791	1.1782
r (SiC_m) (Å)	1.8684	1.8689	1.8690	1.8690	1.8691	1.8692
∠(SiNC) (°)	180.0	170.0	160.0	158.5	150	140.0
∠(NCO) (°)	180.0	178.8	177.5	177.4	176.6	176.0

Table 5
Parameters of the potential energy function for SiNC bending motion for $(CH_3)_3SiNCO$, determined using cc-pVTZ basis set at various levels of theory

	MP2	MP3	MP4	QCISD(T)
H (cm^{-1})	20.7	3.6	7.4	24.6
ρ_e (°)	21.6	13.3	16.5	27.2
f (mdyn Å)	0.023	0.010	0.014	0.024

$$V(\rho) = \frac{Hf(\rho^2 - \rho_e^2)^2}{f\rho_e^4 + (8H - f\rho_e^2)\rho^2}$$

The function is expressed in terms of the coordinate ρ, defined as the supplement of the SiNC angle. It involves three parameters: ρ_e, the equilibrium angle; H, the height of a barrier to linearity of the SiNC chain; and f, the harmonic force constants at $\rho = \rho_e$. The parameters were adjusted in a least squares fit of this function to the total energies calculated with the cc-pVTZ basis sets (Table 6).

The effect of electron correlation on the shape of the SiNC bending potential energy function can be appreciated in Fig. 2. Upon the inclusion of the electron correlation effects, the predicted shape of the potential energy surfaces changes significantly, although the values of the parameters determined at nth order Møller–Plesset do not correlate clearly with such an order n. What we can conclude is that when n even, parameters diminish in a monotonic trend as n rises. The perturbational MP3 and MP4 approach result in the nearly harmonic potential function, whereas at MP2, and also QCISD(T) levels of theory, the function is rather anharmonic, with a very low barrier at the linearity configuration of the SiNCO skeleton. Similar changes were observed for H_3SiNCO with MP3 method, although not with MP4 [12].

5. Vibrational assignment

The present study reports new infrared (for the gas phase and pure liquid), Raman (for the pure liquid) spectra and the INS spectrum (Figs. 3–5) that is used to check and extend the existing assignments. In Table 7 the observed vibrational wavenumbers in each spectrum and the previous assignments from Refs. [14,17] are listed.

In principle, the vibrational assignment was undertaken with the aim of confirming the previous assignments of fundamental modes and to complete those that have not previously been observed. To achieve this, two factors were taken into account: firstly, previous assignments for trimethylsilylisocyanate [16,17] and related molecules [45–48], and secondly, the methods that produced the best molecular geometries. The wavenumbers calculated at MP2/6-311++G** and B3LYP/cc-pVDZ are given in Table 8, where they are compared with the experimental assignments. As a reference the experimental wavenumbers were taken from Raman spectrum because it represents the most complete set of data and, where modes do not appear in the Raman, the corresponding wavenumbers were taken from IR and INS spectra (see Table 8). In Table 1S the calculated wavenumbers of the other theoretical methods used in this work can be found.

Table 6
Total energy of $(CH_3)_3SiNCO$ (cm^{-1}) as a function of SiNCO angle, determined using the cc-pVTZ basis set at various levels of theory[a]

∠(SiNC) (°)	180	170	160	150	140
SCF	0.0	6.69	59.67	175.4	408.4
MP2	0.0	−8.11	−20.28	−3.57	91.23
MP3	0.0	−4.34	3.11	47.50	178.0
MP4	0.0	−5.55	−5.31	28.97	147.0
QCISD (T)	0.0	−10.7	−16.5	−23.2	59.25

[a] Relative to the energy of the linear configuration, calculated with the structural parameters given in Table 4.

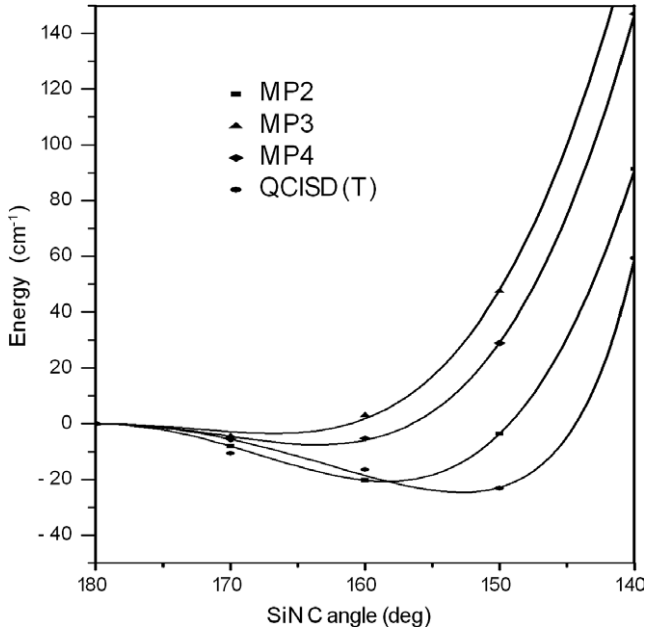

Fig. 2. The relative total energy of trimethylsilylisocyanate as a function the SiNC angle, determined using the cc-pVTZ basis set at various levels of theory.

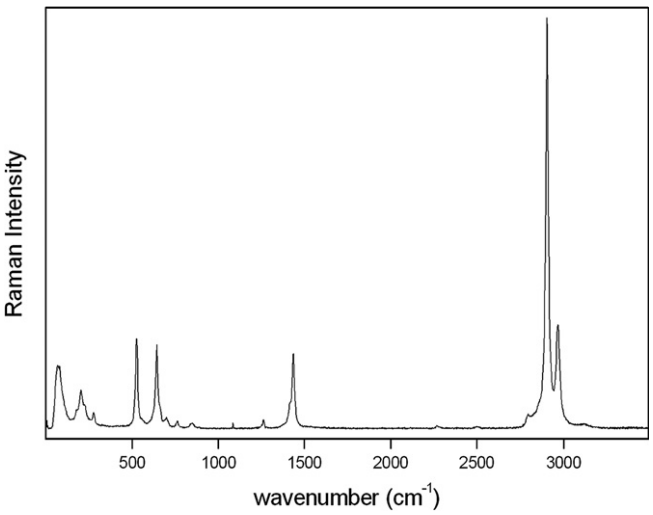

Fig. 3. FT-Raman spectrum of trimethylsilylisocyanate in liquid state.

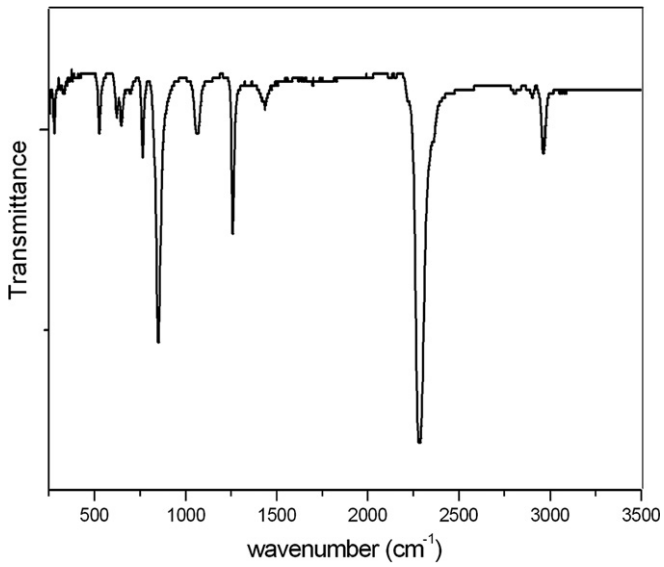

Fig. 4. FT-IR spectrum of trimethylsilylisocyanate in liquid state.

The rms deviation between assigned and calculated wavenumbers for all the methods essayed in this work are included in Table 3. When comparing all the methods using the same basis sets, DFT methods gives better agreement between the observed and calculated vibrational wavenumbers than MP2, although B3LYP and B3PW91 methods show a opposite trend observed in the deviation for the geometrical parameters. Also, when increasing the basis-set size from 6-31G* to 6-311++G** and from cc-pVDZ to cc-pVTZ, a general improvement is observed. The lowest deviation for wavenumbers is obtained from MP2/6-311++G** and DFT/cc-pVTZ, however we have chosen the B3LYP/cc-pVDZ method to perform the vibrational analysis because of minor deviation for angle as has been commented above, and the results have been compared with those obtained from MP2/6-311++G**.

In Fig. 6 the experimental (gas phase) and calculated infrared spectra are shown, the calculated intensities being described by Lorentzian curves (half band width of 2 cm^{-1}) without scaling, for MP2/6-31 G*, MP2/6-311++G**, B3LYP/cc-VDZ and B3PW91/cc-pVTZ methods. DFT gives a reasonable reproduction of the infrared spectrum and is better than the MP2 method in the 500–700 cm^{-1} region and near to 1500 cm^{-1}.

As can be seen in Table 1S, only the modes ν_{18}, ν_{37}, ν_{24} and ν_{42} undergo a clear loss of the degeneration when going from the linear to the bent structure, above all in the case of the MP2 calculations, due to those modes are directly related with the dynamics of the SiNCO skeleton. The modes ν_{24} and ν_{42} have not been assigned up to now due to they appear in the very low energy region, and according to the PED in Table 8, they are not pure modes. However, the modes ν_{18} and ν_{37} are pure and therefore they could be used as a probe to check the evolution of the spectral profile when going from a linear to a bent structure. Furthermore,

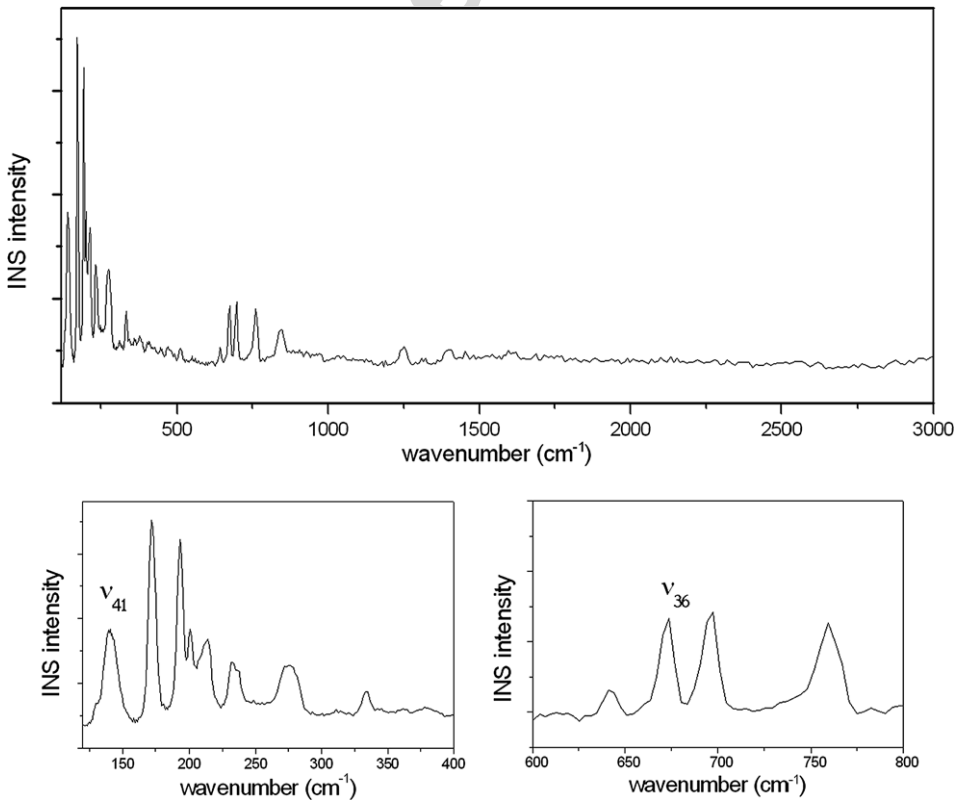

Fig. 5. *Upper:* INS spectrum of trimethylsilylisocyanate; *Lower left*: the INS spectrum of trimethylsilylisocyanate in the region 120–400 cm^{-1}; *Lower right*: the INS spectrum of trimethylsilylisocyanate in the region ~700 cm^{-1}.

Table 7
Vibrational assignments and experimental wavenumbers for $(CH_3)_3SiNCO$ molecule (cm^{-1})

Thayer, Strommen[14]		Durig[16,17]		This work			
IR	Raman	Raman	Assignment	IR liq.[a]	IR gas[a]	INS	Raman[a]
2985	2963	2966	CH_3 stretch asymmetry		2974 w		2973 m
		2966	CH_3 stretch asymmetry				2971 m
		2966	CH_3 stretch asymmetry				2969 m
		2966	CH_3 stretch asymmetry	2964 w	2969 w		2968 m
		2966	CH_3 stretch asymmetry		2965 sh		2967 m
		–	CH_3 stretch asymmetry				2965 m
2915	2901	2903	CH_3 stretch symmetry				2906 vs
		2903	CH_3 stretch symmetry	2904 vw	2910 vw		2904 vs
		2903	CH_3 stretch symmetry				2902 vs
2290		2271	NCO stretch asymmetry	2284 vs	2293 vs		2274 vvw
1435	1435	1435	NCO stretch symmetry	1438 vw	1442 w		1440 mw
		1435	CH_3 symmetric deformation	1436 vw	1437 w		1438 mw
		–	CH_3 symmetric deformation	1423 vw			1433 mw
		–	CH_3 symmetric deformation				1421 vw
1415	1412	1415	CH_3 asymmetric deformation	1419 vw	1419 vw		1420 vw
		1415	CH_3 asymmetric deformation				1418 vw
		–	CH_3 asymmetric deformation			1396	1401 vw
1255	1260	1263	CH_3 asymmetric deformation		1264 m		1265 vw
		1256	CH_3 asymmetric deformation	1258 m			1261 vw
		1256	CH_3 asymmetric deformation			1251	1257 vw
850	850	848	CH_3 rocking	849 s	854 s		853 vw
		848	CH_3 rocking				850 vw
		848	CH_3 rocking			843	844 vw
755	761	763	CH_3 rocking				766 vw
		763	CH_3 rocking	763 w	763 w	759	763 vw
690	701	700	SiC_3 stretch asymmetry	699 vw			704 vw
		700	SiC_3 stretch asymmetry	692 vw	693 vw	698	699 vw
		–	CH_3 rocking	668 vw	668 sh	674	668 sh
642	644	644	SiC_3 stretch symmetry	646 w	647 vw	641	646 mw
616		618	NCO bend	620 w	620 vw		620 vvw
		618	NCO bend				617 vvw
521	528	526	SiN stretching	527 w	536 w	512	529 mw
	117	279	SiC_3 asymmetric deformation	281 w	283 vw		283 vw
		279	SiC_3 asymmetric deformation	278 w	278 vw	276	279 vw
	206	229	SiC_3 symmetric deformation		227 vw	233	229 vw
	287	207	SiC_3 rocking			214	210 w
		207	SiC_3 rocking			200	208 w
		181	CH_3 torsion			193	188 vw
		181	CH_3 torsion			172	184 vw
		–	CH_3 torsion			141	
		–	SiNC bend				
		–	SiNC bend				

[a] v, very; w, weak; m, medium; s, strong; sh, shoulder.

the description of them is similar to the two bending coordinates in two perpendicular planes when the SiNCO moiety is linear. As shown in Fig. 6, the calculated spectral profile from the MP2/6-31G* shows a clear deviation from the experimental one and the difference between the degenerate modes calculated at 593 cm^{-1} and the following one calculated at 660 cm^{-1} (ν_{17}) amount to 67 cm^{-1}. The experimental difference for the above mentioned modes is only 26 cm^{-1}. For the B3LYP/cc-VDZ and B3PW91/cc-pVTZ methods that difference is 31 cm^{-1} and 22 cm^{-1}, respectively. For the MP2/6-311++G** method, the ν_{18} and ν_{37} appear clearly non degenerate in the calculated spectral profile, being the difference between them of 17 cm^{-1}, and the mean difference between those modes and ν_{17} of 55 cm^{-1}. For the B3PW91/cc-pVTZ the loss of the degeneration is almost imperceptible. Therefore, DFT methods, in spite of the NCO angle is calculated farther respect to the electron diffraction than MP2 method, the vibrational spectral profile in the region above discussed is better reproduced.

Note that a strong band at 1074 cm^{-1} is observed in the IR spectrum of the gas phase, but does not appear in the calculated spectra. This band can belong to hexamethyldisiloxane, an impurity that shows a strong absorption at the same wavenumber in the IR gas phase spectrum [49,50].

We have compared the experimental INS spectrum with those calculated for an isolated molecule by using incoherent neutron scattering cross-section and the atomic

Table 8
Observed, calculated and scaling with one (Scaled 1), several scale factors (Scaled 2) and with refined scale factors (Scaled 3) wavenumbers, in cm^{-1}

Mode	Calculated		Observed	Scaled 1[a]	Scaled 2[b]	Scaled 3	Potential energy distribution ($\geqslant 7\%$)	Description
	MP2/6-311++G**	B3LYP/cc-pVDZ						
A′								
ν_1	3167	3118	2971	3004	2991	2978	25 S_7 + 25 S_9 + 25 S_{10} + 25 S_{11}	CH_3 stretch
ν_2	3163	3112	2968	3003	2984	2972	40 S_6 + 13 S_4 + 13 S_5 + 11 S_8 + 11 S_{12}	CH_3 stretch
ν_3	3160	3109	2967	2995	2982	2969	21 S_6 + 20 S_8 + 20 S_{12}	CH_3 stretch
ν_4	3069	3031	2906	2920	2908	2895	19 S_4 + 19 S_5 + 24 S_6	CH_3 stretch
ν_5	3067	3029	2904	2918	2906	2893	11 S_4 + 11 S_5 + 16 S_6 + 12 S_8 + 12 S_{12}	CH_3 stretch
ν_6	2380	2401	2284[IR]	2312	2306	2293	61 S_{14} + 46 S_{15}	NC and CO stretch
ν_7	1482	1476	1440	1422	1430	1435	29 S_{22} + 29 S_{27} + 29 S_{32}	CH_3 asymmetric deformation
ν_8	1476	1446	1438	1393	1381	1427	45 S_{15} + 27 S_{14} + 15 S_{13}	CO and NC stretch
ν_9	1464	1435	1421	1382	1371	1424	54 S_{23} + 18 S_{28} + 11 S_{33}	CH_3 asymmetric deformation
ν_{10}	1444	1422	1396[INS]	1370	1360	1412	33 S_{23} + 32 S_{28} + 32 S_{33}	CH_3 asymmetric deformation
ν_{11}	1319	1279	1265	1232	1279	1265	40 S_{21} + 30 S_{26} + 30 S_{31}	CH_3 symmetric deformation
ν_{12}	1309	1271	1261	1224	1272	1259	61 S_{21} + 20 S_{26} + 20 S_{31}	CH_3 symmetric deformation
ν_{13}	887	867	853	835	845	857	25 S_{30} + 25 S_{35} + 17 S_1	CH_3 rocking
ν_{14}	886	864	850	832	844	857	33 S_{25} + 12 S_2 + 12 S_3 + 8 S_{30} + 8 S_{35}	CH_3 rocking + SiC_3 stretch
ν_{15}	792	774	766	745	752	765	30 S_{24} + 18 S_1 + 8 S_{29} + 8 S_{34}	CH_3 rocking + SiC_3 stretch
ν_{16}	717	694	704	668	683	697	31 S_1 + 28 S_{24} + 8 S_{29} + 8 S_{34} + 7 S_2 + 7 S_3	SiC_3 stretch + CH_3 rocking
ν_{17}	664	635	646	611	641	654	24 S_2 + 24 S_3 + 20 S_1 + 18 S_3	SiC_3 stretch
ν_{18}	617	603	620	581	601	606	99 S_{37}	NCO bending[d]
ν_{19}	532	511	529	492	516	525	61 S_{13} + 8 S_{14}	SiN stretch
ν_{20}	269	263	283	254	287	284	76 S_{19} + 19 S_{17}	SiC_3 rocking
ν_{21}	215	216	229	208	233	231	77 S_{16} + 8 S_{24} + 8 S_{29} + 8 S_{34}	SiC_3 symmetric deformation
ν_{22}	190	189	208	182	205	204	63 S_{18} + 29 S_{20}	SiC_3 asymmetric deformation
ν_{23}	172	162	188	156	148	178	46 S_{39} + 46 S_{40}	CH_3 torsion
ν_{24}	42	26	–	25	26	26	65 S_{36} + 25 S_{37}	SiNC bending
A″								
ν_{25}	3169	3119	2973	3005	2992	2978	45 S_4 + 45 S_5	CH_3 stretch
ν_{26}	3167	3118	2969	3003	2990	2977	20 S_7 + 25 S_9 + 20 S_{10} + 24 S_{11}	CH_3 stretch
ν_{27}	3159	3108	2965	2994	2982	2968	30 S_8 + 30 S_{12} + 13 S_7 + 13 S_{10}	CH_3 stretch
ν_{28}	3067	3029	2902	2918	2905	2893	15 S_7 + 20 S_8 + 14 S_9 + 15 S_{10} + 14 S_{11} + 20 S_{12}	CH_3 stretch
ν_{29}	1475	1435	1433	1383	1371	1424	39 S_{28} + 46 S_{33}	CH_3 asymmetric deformation
ν_{30}	1463	1428	1419	1376	1365	1417	43 S_{27} + 42 S_{32} + 8 S_{23}	CH_3 asymmetric deformation
ν_{31}	1461	1428	1418	1375	1365	1417	58 S_{22} + 14 S_{27} + 15 S_{32}	CH_3 asymmetric deformation
ν_{32}	1307	1270	1257	1224	1271	1258	50 S_{26} + 50 S_{31}	CH_3 symmetric deformation
ν_{33}	886	864	844	832	841	854	21 S_{24} + 20 S_{29} + 20 S_{34} + 9 S_{16}	CH_3 rocking
ν_{34}	790	772	763	744	751	765	22 S_{29} + 22 S_{34} + 15 S_2 + 14 S_3	CH_3 rocking + SiC_3 stretch
ν_{35}	713	691	699	666	680	694	21 S_2 + 21 S_3 + 23 S_{29} + 23 S_{34}	SiC_3 stretch + CH_3 rocking
ν_{36}	696	689	674[INS]	664	651	664	38 S_{25} + 38 S_{30} + 38 S_{35}	CH_3 rocking
ν_{37}	600	601	617	578	600	617	100 S_{42}	NCO bending[d]
ν_{38}	265	260	279	250	283	281	77 S_{20} + 20 S_{18} + 10 S_{25}	SiC_3 rocking
ν_{39}	193	190	210	183	206	205	61 S_{17} + 28 S_{19}	SiC_3 asymmetric deformation
ν_{40}	168	160	184	155	147	176	48 S_{38} + 21 S_{39} + 21 S_{40}	CH_3 torsion
ν_{41}	138	142	141[INS]	137	130	156	49 S_{38} + 26 S_{39} + 26 S_{40}	CH_3 torsion
ν_{42}	8	11	–	11	11	11	64 S_{41} + 34 S_{20}	SiC_3 torsion
rms	93.2	69.8		30.4	25.2	7.1		

P.E.D. corresponding to Scaled 3 and description for the trimethylsilylisocyanate molecule.
[a] By 0.928 from Ref. [38].
[b] By scale factors transfering from Ref. [39].
[c] From refinement of multiple scale factors.
[d] The description of these two modes is similar to the two bending coordinates in two perpendicular planes when the SiNCO moiety is linear.

displacements matrices at each level of theory and, in this way, we can establish which method best reproduces the INS spectrum as a whole. The limit for the external modes was fixed at 120 cm^{-1}, which actually includes the normal modes ν_{24} and ν_{42} that are calculated below 100 cm^{-1}. Figs. 1S and 2S show the effect of the basis set for the MP2 and

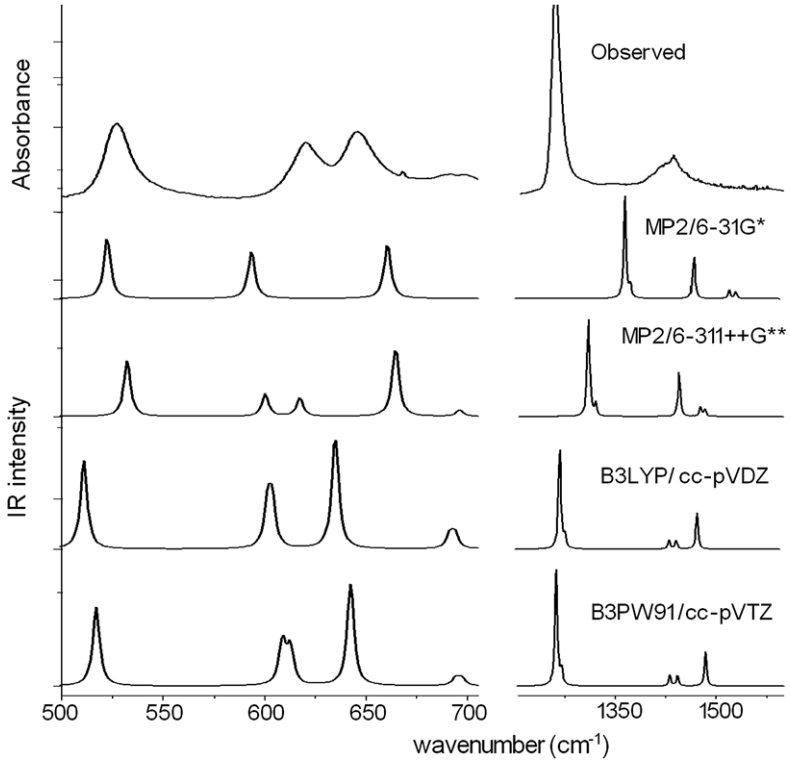

Fig. 6. Observed and calculated IR spectra of the $(CH_3)_3SiNCO$ molecule.

B3LYP methods, and Fig. 7 shows the calculated INS spectra from the all methods with cc-pVTZ basis set and also MP2 with some basis sets that gave a bent skeleton SiNCO. In general, there are some differences in the positions and the intensities of the normal modes, but the predictions using the isolated molecule approximation agree well with those measured in the crystal in the 120–250 cm^{-1} region. An expansion of this region is illustrated in Fig. 8. In this low-frequency region intermolecular interactions are expected to play an important role, and it is surprising that agreement is so good.

Although the potential that describes the rotational dynamics of a methyl group is determined by intermolecular interactions with the neighbouring atoms [19], for tetramethyl compounds of silicon, germanium, tin and lead the rotational potential is mainly of intramolecular origin. The methyl group reorientation is primarily hindered by neighbouring methyl groups of the same molecule [51]. For the $Sn(CH_3)_4$ molecule, the torsion region in INS spectrum looks rather similar to what we have seen in trimethylsilylisocyanate and we suggest that as in $Sn(CH_3)_4$, it is the intramolecular interactions that determine the rotational potential. The structure analysis of $(CH_3)_4Sn$ [52] revealed unambiguously the existence of two inequivalent types of methyl groups with relative weights 3:1, the CH_3 group oriented along the threefold axis being different to other three equivalent CH_3 groups. The rotational motion of the unique group is hindered by a compression of the $Sn(CH_3)_4$ tetrahedron along its axis, leading to a shorter distance to the neighbouring atoms.

Trying to go further from the isolated molecule approximation and starting from the crystal structure already determined at 183 K [53], the theoretical solid structure of trimethylsilyl isocyanate has been analysed by using VASP and DMOL3 codes, implementing DFT methods, however none of them gave good agreement with the INS observed spectrum pointing out that there may be something wrong with the solid structure and thus it could be necessary to redetermine it.

5.1. Assignment of bands for Me_3SiNCO

5.1.1. Assignments above 1250 cm^{-1}

The CH_3 stretching modes give rise to two groups of bands observed in Raman spectrum around 2969 and 2904 cm^{-1}, the second group being more intense (see Fig. 3). According to our calculations, these modes are 100% C–H stretching.

The N–C and C–O stretching modes are very mixed showing two bands with different contribution of each stretch type. The strong band in the infrared spectrum of the liquid at 2284 cm^{-1} has been assigned to the normal mode ν_6, in which the N–C stretch contributes more than the C–O stretch due to the difference in atomic mass, this being in agreement with the calculations. The second N–C and C–O stretching mode has been observed at 1438 cm^{-1} in the Raman spectrum and shows a larger C–O stretch contribution although the Si–N stretch also contributes significantly.

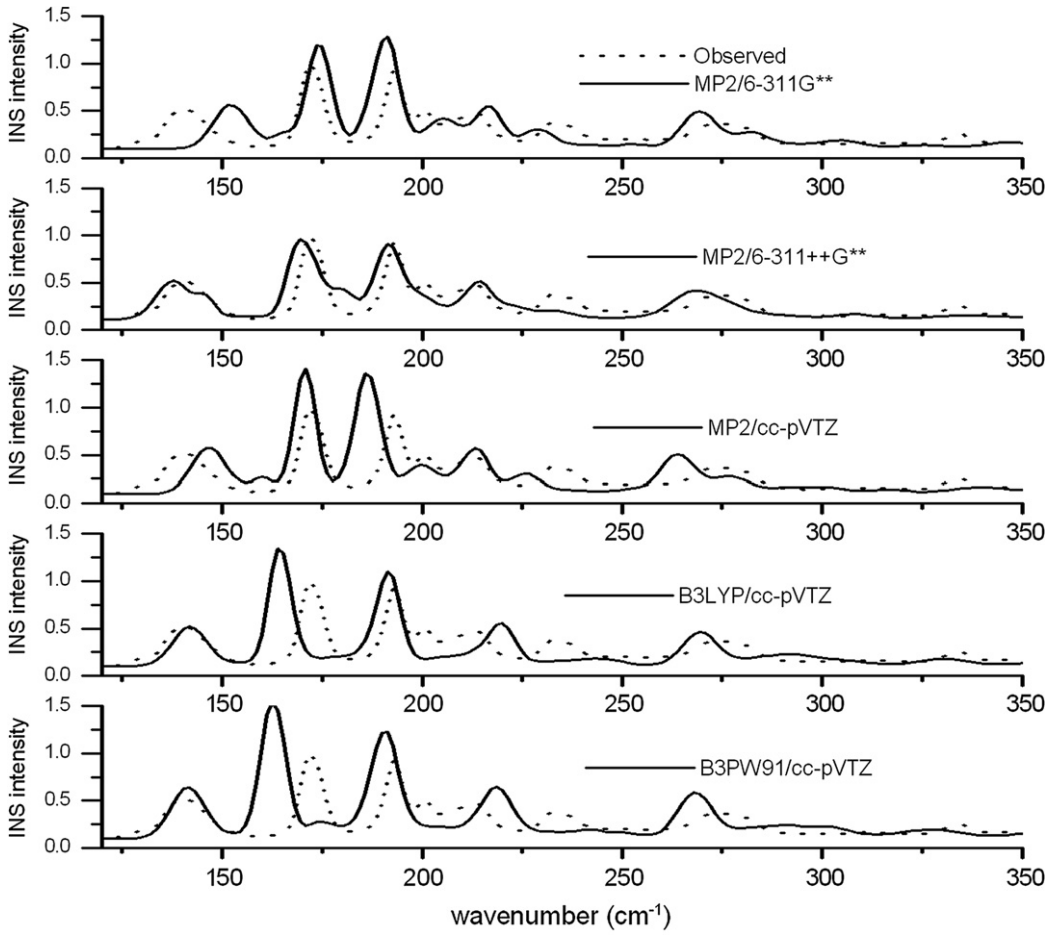

Fig. 7. Observed (dotted line) and calculated (solid line) INS spectra of $(CH_3)_3SiNCO$ for the vibrational wavenumbers and atomic displacement at several levels of theory.

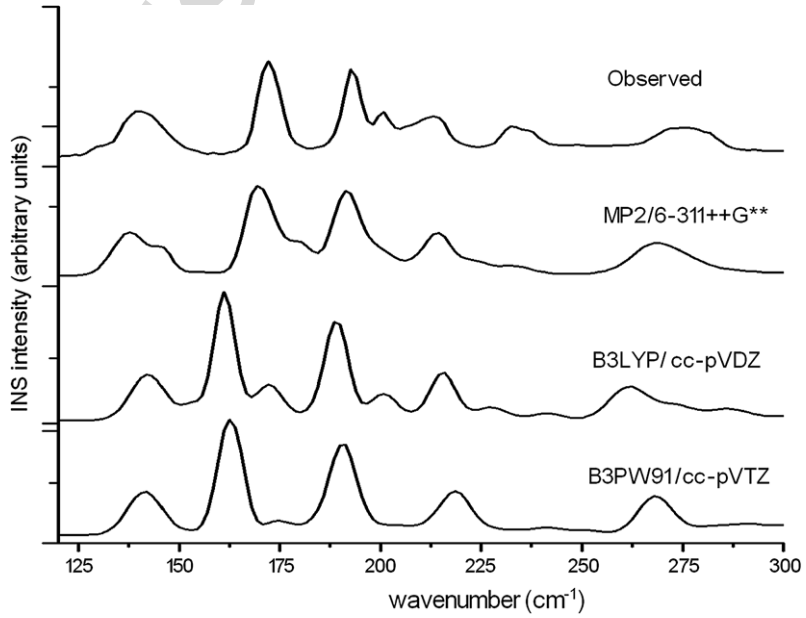

Fig. 8. Comparison of observed INS spectrum with calculated spectra using different methods.

According to our calculations, the CH_3 antisymmetric deformation modes should occur in the 1400–1500 cm^{-1} region. A relatively intense band in the Raman spectrum of the liquid is observed at 1438 cm^{-1} with two shoulders at about 1440 cm^{-1} and 1433 cm^{-1}. These two shoulders were assigned to the CH_3 antisymmetric deformation. In a previous study [17], it was difficult to distinguish between antisymmetric and symmetric deformations, the CH_3 symmetric deformations being calculated at higher wavenumbers than the CH_3 antisymmetric and the observed band at 1435 cm^{-1} was assigned to CH_3 symmetric bending mode.

A triplet in the Raman spectrum appears around 1419 cm^{-1} which, according to our calculations, corresponds to the other CH_3 antisymmetric deformations. This assignment is in agreement with the band assigned at 1415 cm^{-1} by Durig [16].

The last CH_3 antisymmetric bending mode, which is not observed in Raman or infrared spectra, is assigned near to 1400 cm^{-1} in INS spectrum. This mode has not been assigned before although previous works showed calculated values of 1416 cm^{-1} and 1407 cm^{-1} for the $(CH_3)_3SiNCO$ and $(CH_3)_3SiH$ molecules, respectively [17,45] which agree with our calculations.

Bands in the Raman spectrum that appear in the 1265–1255 cm^{-1} region are be assigned to the CH_3 symmetric deformations. According to our calculations, three modes are predicted at 1265 cm^{-1}, 1259 cm^{-1} and 1258 cm^{-1} and they have a contribution of the 100% to the deformation of the methyl groups. Thus, the bands observed at 1265 cm^{-1}, 1261 cm^{-1} and 1257 cm^{-1} in the Raman spectrum have been assigned to ν_{11}, ν_{12} and ν_{32}, respectively.

5.1.2. Assignments between 850–500 cm^{-1}

In agreement with Durig's work, our calculations predict the CH_3 rocking modes in the range 850–765 cm^{-1}, these being mixed mainly with the SiC_3 stretching. Furthermore, a new rocking mode has been calculated, with a contribution of more than 95% due to the methyl rocking vibrations, which is assigned at 674 cm^{-1} in the INS spectrum (see Fig. 5). This feature is rather weak in IR and Raman spectra where it is only observed as a weak shoulder on a band of medium-weak intensity at 668 cm^{-1} (see Table 7). This mode at 674 cm^{-1} was not previously assigned by Durig because it belongs to the A_2 block assuming C_{3v} symmetry for the molecule and it is forbidden by selection rules in optical spectroscopies.

Skeletal vibrations of the $(CH_3)_3SiNCO$ molecule are observed in Raman spectrum as a double band around 700 cm^{-1} and a further more intense feature at 646 cm^{-1}. These are assigned to SiC_3 stretching modes although they are mixed with other vibrations. Similarly, the assignment of the NCO bending and SiNCO torsion modes to a very weak double band at 620 (infrared and Raman) and 617 cm^{-1} (Raman) were confirmed by taking into account the calculated wavenumbers and their 100% contribution to these modes. However, the Raman band at 529 cm^{-1}, which has been assigned by Durig at 526 cm^{-1} to the Si–N stretching, it is calculated as being highly mixed with the SiC_3, N–C and C–O stretches. This Si–N stretch was previously assigned at 570 cm^{-1} in H_3SiNCO [46], 492 cm^{-1} in H_3SiNCS [46] and 475 cm^{-1} in $(CH_3)_3SiNCS$ [17].

5.1.3. Assignments below 300 cm^{-1}

In this region, the skeletal bending modes are expected to arise between 280 and 210 cm^{-1}, and are calculated as a mixture with CH_3 rocking vibrations. Thus, two SiC_3 rocking are assigned to the bands observed at 283 (ν_{20}) and 279 cm^{-1} (ν_{38}) in the Raman spectrum. The SiC_3 symmetric deformation, ν_{21}, is assigned to a rather weak band observed at 229 cm^{-1} in the Raman. Corresponding bands are observed at 227 cm^{-1} and 233 cm^{-1} in the IR and INS spectra, respectively. This assignment is in agreement with the band assigned at 228 cm^{-1} to the SiC_3 symmetric deformation in the $(CH_3)_3SiCl$ [47]. In addition, according to our calculations two SiC_3 antisymmetric bending modes have been assigned at a double band around 209 cm^{-1} and they are in excellent accord with the assignment of

Table 9
Scaling factors for the different types of natural internal coordinates in trimethylsilylisocyanate

No.	Mode	MP2/6-311++G**		B3LYP/cc-pVDZ			
		Initial value	After refinement	Initial value	After refinement	Initial value[39]	After refinement
1	C–Si and N-Si stretching	1.0	0.981	1.0	1.084	1.042	1.084
2	C–H stretching	1.0	0.886	1.0	0.912	0.920	0.912
3	N–C and C–O stretching	1.0	0.922	1.0	0.911	0.922	0.911
4	C–Si–C and C–Si–N bending	1.0	1.160	1.0	1.187	1.218	1.187
5	H–C–H and H–C–Si bending (CH_3 symmetric deformation)	1.0	0.922	1.0	0.977	1.000	0.977
6	H–C–H bending (CH_3 asymmetric deformation)	1.0	0.947	1.0	0.988	0.915	0.988
7	H–C–Si bending (CH_3 rocking)	1.0	0.894	1.0	0.926	0.890	0.926
8	Si–N–C bending	1.0	1.000	1.0	1.000	1.000	1.000
9	N–C–O bending	1.0	1.012	1.0	1.050	0.990	1.050
10	CH_3 torsion	1.0	1.149	1.0	1.202	0.831	1.202
11	C–Si–N–C torsion	1.0	1.000	1.0	1.000	1.000	1.000
12	Si–N–C–O torsion	1.0	1.058	1.0	1.057	1.000	1.057

Table 10
Root-mean square deviation, in cm^{-1}, between the experimental and calculated wavenumbers for $(CH_3)_3SiNCO$ molecule

Method		r.m.s.
MP2/6-311++G**	Unscaled	93.16
	Scaled with one scale factor (0.9025)	37.89
	Refined the scale factors (initial s.f. = 1.0)	7.94
B3LYP/cc-pVDZ	Unscaled	69.85
	Scaled with one scale factor (0.928)	30.37
	Scaled with scale factors. transferring from Ref. [39]	25.24
	Refined the scale factors (initial s.f. = 1.0)	7.06
	Refined the scale factors transferring from Ref. [39]	7.06

these vibrations in other molecules such as trimethylsilane [45] or trimethylsilanol [48], where this mode was assigned at 208 and 209 cm^{-1}, respectively. However, Durig attributed this band at 207 cm^{-1} to SiC_3rocking [16].

Three of the torsional modes of methyl group have been observed at 188, 184 (both in Raman spectrum) and 141 cm^{-1} (in INS spectrum). Two of these are calculated to be mixed with another CH_3 vibrations but the band at 141 cm^{-1} that corresponds to the ν_{41} normal mode is 100% CH_3 torsional mode. This has not been assigned previously since under C_{3v} symmetry it belongs to A_2 block and it is optically-inactive mode.

The SiNC bending and SiC_3 torsion have not been assigned because they cannot be separated from the lattice modes in the INS spectrum and they are absent from in the IR and Raman spectra.

5.2. Force field calculations

For the scaling of the force fields resulting at the B3LYP/cc-pVDZ and MP2/6-311++G** levels of theory, a set of ten scale factors was defined taking account the different kind of natural coordinates. In a first step, the vibrational wavenumbers were predicted using a unique value for all the scale factors, as proposed in reference [38] for B3LYP and MP2 methods, 0.928 and 0.9025, respectively. In a second step, the scale factors values recommended by Kalincsák and Pongor [39] for the B3LYP/6-31G* method were transferred to the force constant matrix calculated at the B3LYP/ccVDZ level (when it was not possible we took the unity). Observed and calculated wavenumbers from the B3LYP/cc-pVDZ scaled force fields described previously are collected in Table 8.

In order to reproduce the 40 assigned experimental wavenumbers, a least squares refinement was made on the basis of the difference between observed and calculated wavenumbers. As the modes ν_{24} and ν_{42} are not assigned, scaling factors for the corresponding force constants, F_{41} and F_{36}, were constrained to unity. We tried two options: (a) starting from unity for all scale factors and (b) from ten scale factors transferred as mentioned above, this last only in the case of the B3LYP method. The initial and final scale factors corresponding to the MP2/6-311++G** and B3LYP/cc-pVDZ methods are listed in Table 9 wherein it can be seen that the scale factors refined with DFT methods are, as is expected, the same for two initial possibilities, a and b. All scale factors are in the range 0.9–1.1, except for the CH_3 torsion and SiC_3 deformation. The resulting wavenumbers from the refinement to the experimental data from B3LYP/cc-pVDZ, potential energy distribution and root mean square (r.m.s) values are collected in Table 8.

We can conclude that the rms obtained comparing the experimental and theoretical wavenumbers (see Table 10) from B3LYP/cc-pVDZ and MP2/6-311++G** methods are 69.9 cm^{-1} and 93.2 cm^{-1}, respectively. These were reduced to 30.4 cm^{-1} and 37.9 cm^{-1}, when using only one scale factor, and further reduced to 7.1 cm^{-1} and 7.9 cm^{-1} when the scale factors were refined. However, when the 10 different scale factors are transferred from reference 39 for the B3LYP method, the rms varies from an initial value of 25.2 cm^{-1} to a final value of 7.1 cm^{-1} when they were refined.

The initial and final force constants after refining the scale factors for B3LYP and MP2 calculations appear in Table 11. The force constant values are compared with those reported for trimethylsilylisocyanate and related molecules. In general, the results agree for analogous force constants and the values of the N–C and C–O stretching force constants are in the range 13.7–15.0 mdyn $Å^{-1}$. Moreover, the values for N–C stretching in our work are somewhat longer than the value for C–O stretching force constant, which is in agreement with the values from the scaled quantum mechanical force field performed by Sullivan et al. for methylisocyanate [54]. However, the values proposed for the N–C and C–O stretching force constants from the empirical force field when studying $(CH_3)_3SiNCO$ [17] and also similar compounds [56,57] are reversed, that is, N–C stretching being somewhat smaller than the values for C–O stretching force constants.

6. Conclusions

The optimized equilibrium structure of the $(CH_3)_3$-SiNCO molecule is linear o bent depending on the level of theory. For MP2 and the density functionals, B3LYP and B3PW91, implementing with large basis sets, SiNCO skeleton is bent and the calculated energy values are closer to those arising from electron diffraction geometries. The

Table 11
Force constants in internal (valence) coordinates for $(CH_3)_3SiNCO$ molecule

Force constant	$(CH_3)_3SiNCO$ this work				$(CH_3)_3SiNCX$[a]		H_3SiNCO[c]	H_3GeNCO[d]	H_3CNCO[e]
	MP2/6-311++G**		B3LYP/cc-pVDZ		X=O	X=S			
	Initial	Scaled SQM	Initial	Scaled SQM					
$F_{1,1}$ - $F_{3,3}$ (Si–C)	3.178–3.130	3.301–3.252	2.864 – 2.841	3.081–3.105	2.703	2.703			
$F_{4,4}$ - $F_{12,12}$ (C–H)	5.430–5.389	4.772–4.808	5.227 – 5.269	4.768–4.807	4.728	4.728			
$F_{13,13}$ (Si–N)	3.955	4.109	3.737	4.053	4.113	3.991	4.352	3.12	
$F_{14,14}$ (N–C)	15.114	13.878	16.077	14.644	13.75[b]	13.75[b]	11.22	13.73	16.46
$F_{15,15}$ (C–O)	14.955	13.731	15.145	13.794	15.00[b]		16.06	15.66	16.04
$F_{13,14}$	0.095	0.092	0.129	0.128	0.403	0.425			
$F_{14,15}$	0.791	0.726	1.159	1.056	1.414				1.832
$F_{16,16}$ (SiC_3 deformation)	0.824	0.966	0.821	0.974					
$F_{17,17}$, $F_{18,18}$ (C–Si–C)	0.635, 0.636	0.744, 0.746	0.622, 0.620	0.738, 0.736	0.877	0.877			
$F_{19,19}$, $F_{20,20}$ (C–Si–N)	0.765, 0.725	0.896, 0.849	0.761, 0.728	0.903, 0.864	0.443	0.503			
$F_{21,21}$, $F_{26,26}$, $F_{31,31}$ (CH_3 deformation)	0.484 – 0.485	0.445–0.446	0.465	0.454					
$F_{22,22}$, $F_{23,23}$, $F_{27,27}$, $F_{28,28}$, $F_{32,32}$, $F_{33,33}$ (H–C–H)	0.560–0.562	0.531–0.533	0.539–0.541	0.532–0.534	0.566–0.430	0.566–0.430			
$F_{24,24}$, $F_{25,25}$, $F_{29,29}$, $F_{30,30}$, $F_{34,34}$, $F_{35,35}$ (H–C–Si)	0.400–0.409	0.344–0.352	0.397–0.402	0.368–0.373	0.467–0.386	0.467–0.386			
$F_{36,36}$ (Si–N–C)	0.046	0.046	0.029	0.029	0.044	0.058	0.012		
$F_{37,37}$ (N–C–O)	0.760	0.763	0.761	0.798	0.630		1.011	0.66–0.71	0.754–0.737
$F_{38,38}$- $F_{40,40}$ (CH_3 torsion)	0.049, 0.048	0.055–0.056	0.044, 0.046	0.053, 0.055					
$F_{41,41}$ (SiC_3 torsion)	0.0003	0.0003	0.0003	0.0003					
$F_{42,42}$ (Si–N–C–O torsion)	0.0018	0.0019	0.0008	0.0008					

Units are mdyn $Å^{-1}$ for stretchings and strech-strech interactions and mdyn Å rad^{-2} for angular deformations.

[a] Ref. [17].

[b] Ref. [55].

[c] Ref. [56] (Refined force constants from B3LYP/6-31G*).

[d] Ref. [57] (Valence field force constants).

[e] Ref. [54] (MP2/6-31G** scaled).

research of the potential energy surface of SiNC bending allow us to conclude about the effect of electron correlation on the shape of SiNC bending potential energy function which is rather anharmonic at MP2 and QCIS(D) level of theory.

A complete vibrational analysis has been performed by combining infrared, Raman and inelastic neutron scattering techniques and ab initio and DFT calculations. The normal coordinates analysis has been carried out by scaling the force fields calculated at MP2/6-311++G** and B3LYP/cc-pVDZ levels of theory by following the scaled quantum mechanical force field (SQMFF) methodology. Finally, in order to obtain the best agreement between calculated and observed vibrational wavenumbers, the scale factors were refined by least squares yielding a final r.m.s. of $\approx 7\ cm^{-1}$.

In this work, a reassignment of several bands, i.e. methyl deformations and SiC_3 deformation has been made and two of the modes that are silent in optical spectroscopies under the C_{3v} symmetry (A_2) have been assigned using the INS spectrum at 674 cm^{-1} and 141 cm^{-1}. In these systems the agreement between the INS spectra for the crystal and calculations for the isolated molecule is quite good, this being unusual in the low-frequency region where the intermolecular interactions are usually dominant.

Acknowledgements

We are grateful to ISIS for enabling us to record the INS spectrum and the European Community for providing financial support. The authors thank A. Garzón (University of Castilla-La Mancha) for his kind help with some calculations. The research grants of CIUNT (Consejo de Investigaciones de la Universidad Nacional de Tucumán) and CONICET (Consejo Nacional de Investigaciones Científicas y Técnicas) are gratefully acknowledged.

Appendix A. Supplementary data

Supplementary data associated with this article can be found, in the online version, at doi:10.1016/j.chemphys.2006.07.033.

References

[1] A. Hosomi, K. Miura, Bull. Chem. Soc. Jap. 77 (5) (2004) 835.
[2] A.S. Maria Chong, X.S. Zhao, A.T. Kustedjo, S.Z. Qiao, Micropor. Mesopor. Mater. 72 (2004) 33.
[3] H. Meier, D. Ickenroth, U. Stalmach, K. Koynov, A. Bahtiar, C. Bubeck, Eur. J. Org. Chem. 23 (2001) 443.
[4] P. Kapferer, V. Birault, J.F. Poisson, A. Vasella, Helv. Chim. Acta 86 (6) (2003) 2210.
[5] G.A. Chmutova, V.V. Zverev, M.A. Pudovik, N.A. Khailova, A.N. Pudovik, Russ. J. Gen. Chem. 73 (11) (2003) 1696.
[6] I.L. Nikolaeva, A.R. Burilov, D.I. Kharitonov, N.E. Krepysheva, M.A. Pudovik, A.I. Konovalov, Russ. J. Gen. Chem. 72 (2) (2002) 232.
[7] K. Kimura, K. Katada, S.V. Bauer, J. Am. Chem. Soc. 88 (3) (1966) 416.
[8] A.J. Careless, M.C. Green, H.W. Kroto, Chem. Phys. Lett. 16 (2) (1972) 414.
[9] S. Cradock, C.M. Huntley, J.R. Durig, J. Mol. Struct. 127 (1985) 319.
[10] M.H. Palmer, A.D. Nelson, J. Mol. Struct. 689 (2004) 161.
[11] C. Zanchini, A. Crispín, J. Mol. Struct. (Theochem) 682 (2004) 17.
[12] J. Koput, Chem. Phys. Lett. 259 (1996) 661.
[13] D.E. Woon, T.H. Dunning Jr., J. Chem. Phys. 99 (1993) 1914.
[14] J.S. Thayer, D.P. Strommen, J. Organomet. Chem. 5 (1966) 383.
[15] D. Paulin, I. Widmaier, Z. Anorg. Allg. Chem. 300 (1959) 194.
[16] J.R. Durig, J.F. Sullivan, A.W. Cox Jr., B.J. Streusand, Spectrochim. Acta 34A (1978) 719.
[17] J.R. Durig, M. Jalillan, Appl. Spectrosc. 33 (4) (1979) 364.
[18] P. Pulay, G. Fogarasi, G. Pongor, J.E. Boggs, A. Vargha, J. Am. Chem. Soc. 105 (1983) 7037.
[19] M. Prager, H. Grim, A. Desmedt, R.E. Lechner, Chem. Phys. 292 (2003) 161.
[20] M.R. Johnson, M. Prager, H. Grimm, M.A. Neuman, G.J. Kearley, C.C. Wilnson, Chem. Phys. 244 (1999) 47.
[21] L. van Eijck, M.R. Johnson, G.J. Kearley, J. Phys. Chem. A 107 (2003) 8980.
[22] M.J. Frisch, G.W. Trucks, H.B. Schlegel, G.E. Scuseria, M.A. Robb, J.R. Cheeseman, J.A. Montgomery Jr., T.Vreven, K.N. Kudin, J.C. Burant, J.M. Millam, S.S. Iyengar, J. Tomasi, V. Barone, B. Mennucci, M. Cossi, G. Scalmani, N. Rega, G.A. Petersson, H. Nakatsuji, M. Hada, M. Ehara, K. Toyota, R. Fukuda, J. Hasegawa, M. Ishida, T. Nakajima, Y. Honda, O. Kitao, H. Nakai, M. Klene, X. Li, J.E. Knox, H.P. Hratchian, J.B. Cross, C. Adamo, J. Jaramillo, R. Gomperts, R.E. Stratmann, O. Yazyev, A.J. Austin, R. Cammi, C. Pomelli, J.W. Ochterski, P.Y. Ayala, K. Morokuma, G.A. Voth, P. Salvador, J.J. Dannenberg, V.G. Zakrzewski, S. Dapprich, A. D. Daniels, M.C. Strain, O. Farkas, D.K. Malick, A.D. Rabuck, K. Raghavachari, J.B. Foresman, J.V. Ortiz, Q. Cui, A.G. Baboul, S. Clifford, J. Cioslowski, B.B. Stefanov, G. Liu, A. Liashenko, P. Piskorz, I. Komaromi, R.L. Martin, D.J. Fox, T. Keith, M.A. Al-Laham, C.Y. Peng, A. Nanayakkara, M. Challacombe, P.M.W. Gill, B. Johnson, W. Chen, M.W. Wong, C. Gonzalez, J.A. Pople, Gaussian, Inc., Pittsburgh PA, 2003.
[23] J. Hehre, L. Random, P.V.R. Scheleyer, J.A. Pople, Ab initio Molecular Orbital Theory, Wiley, New York, 1986.
[24] T.H. Dunning Jr., J. Chem. Phys. 90 (1989) 1107.
[25] D.E. Woon, T.H. Dunning Jr., J. Chem. Phys. 98 (1993) 1358.
[26] R.A. Kendall, T.H. Dunning Jr., R.J. Harrison, J. Chem. Phys. 96 (1992) 6796.
[27] D.J. Becke, Chem. Phys. 98 (1993) 5648.
[28] C. Lee, W. Yang, R.G. Parr, Phys. Rev. B 37 (1988) 785.
[29] B. Miehlich, A. Savin, H. Stoll, H. Preuss, Chem. Phys. Lett. 157 (1989) 200.
[30] P.J. Perdew, Y. Yang, Phys. Rev. B45 (1992) 13244.
[31] G.J. Kearley, J. Chem. Soc. Faraday Trans. II 82 (1986) 41.
[32] J. Howard, C.B. Boland, J. Tomkinson, Chem. Phys. 77 (1983) 145.
[33] J. Tomkinson, M. Warner, A.D. Taylor, Mol. Phys. 51 (1984) 381.
[34] J.A. Pople, M. Head-Gordon, K. Raghauachari, J. Chem. Phys. 87 (1987) 5968.
[35] E. Martínez Torres, VIBRA, versión 1.0; Universidad de Castilla-La Mancha, Ciudad Real, Spain, 1997.
[36] L. Hedberg, I.M. Mills, J. Mol. Spectrosc. 160 (1993) 117.
[37] G. Fogarasi, X. Zhou, P.W. Taylor, P. Pulay, J. Am. Chem. Soc. 114 (1992) 8191.
[38] G. Rauhut, P. Pulay, J. Phys. Chem. 99 (10) (1995) 3093.
[39] F. Kalincsák, G. Pongor, Spectrochim. Acta 58A (2002) 999.
[40] J.A. Duckett, A.G. Robiette, M.C.L. Gerry, J. Mol. Spectrosc. 90 (1981) 374.
[41] C. Glidewell, A.G. Robiette, G.M. Sheldrick, Chem. Phys. Lett. 16 (1972) 526.
[42] J.D. Murdock, D.W.H. Rankin, B. Beagley, J. Mol. Struct. 31 (1976) 291.
[43] R.W. Kilb, L. Pierce, J. Chem. Phys. 27 (1957) 108.
[44] L. Pierce, D.H. Petersen, J. Chem. Phys. 33 (3) (1960) 907.
[45] D.C. McKean, Spectrochim. Acta A55 (1999) 1485.

[46] J.R. Durig, J.S. Church, J. Chem. Phys. 73 (10) (1980) 4784.
[47] M. Montejo, F. Partal Ureña, F. Márquez, I.S. Ignatyev, J.J. López González, Spectrochim. Acta A62 (2005) 293.
[48] I.S. Ignatyev, F. Partal, J.J. López González, T. Sundius, Spectrochim. Acta A60 (2004) 1169.
[49] K. Hammada, H. Morishita, Spectrosc. Lett. 16 (1983) 717.
[50] P.J. Linstrom, W.G. Mallard, (Ed.), NIST Chemistry WebBook, NIST Standard Reference Database Number 69, National Institute of Standard and Technology, Gaithersburg MD, 2003.
[51] W. Müller-Warmuth et al., Z. Naturforsch 39a (1984) 66.
[52] M. Prager, K.-H. Duprée, W. Müller-Warmuth, Z. Phys. B-Condensed Matter 51 (1983) 309.
[53] A.I. Gusev, E.B. Chuklanova, A.S. Zhdanov, E.V. Muzovskaya, V.P. Kozyukov, Zh. Strkt. Khim. 30 (1989) 182.
[54] J.F. Sullivan, H.L. Heusel, W.M. Zunic, J.R. Durig, Spectrochim. Acta 50A (3) (1994) 435.
[55] R.G. Lett, W.H. Flygare, J. Chem. Phys. 47 (1967) 4730.
[56] A. Navarro, M.P. Fernández-Liencres, A. Ben Altabef, M. Fernández Gómez, J.J. López González, R. Escribano, J. Mol. Struct. 482-483 (1999) 601.
[57] J.F. Sullivan, J.R. Durig, J. Mol. Struct. 60 (1980) 37.